RC23518 (W0501-134) January 27, 2005
Electrical Engineering

IBM Research Report

Efficient Modeling Methodology and Hardware Validation of Glass-Ceramic Based Wiring for High-Performance Single- and Multi-Chip Modules

Sungjun Chun, Anand Haridass, Alina Deutsch[1], Barry Rubin[1], Christopher Surovic[1], Erich Klink[2], Daniel O'Connor[3], Hsichang Liu[3], Christopher Spring[3], Thomas-Michael Winkel[2], Warren Dyckman[3], George Katopis[3], Gerard Kopcsay[1]

IBM System and Technology Group
11400 Burnet Road
Austin, TX 78758

[1]IBM Research Division
Thomas J. Watson Research Center
P.O. Box 218
Yorktown Heights, NY 10598

[2]IBM System and Technology Group
Boeblingen, Germany

[3]IBM System and Technology Group
East Fishkill, NY

Research Division
Almaden - Austin - Beijing - Haifa - India - T. J. Watson - Tokyo - Zurich

Efficient Modeling Methodology and Hardware Validation of Glass-Ceramic Based Wiring for High-Performance Single- and Multi-Chip Modules

Sungjun Chun, Anand Haridass, Alina Deutsch[1], Barry Rubin[1], Christopher Surovic[1], Erich Klink[2], Daniel O'Connor[3], Hsichang Liu[3], Christopher Spring[3], Thomas-Michael Winkel[2], Warren Dyckman[3], George Katopis[3], Gerard Kopcsay[1]

IBM System and Technology Group, 11400 Burnet Rd, Austin, TX 78758
Email: {sungjun, anandh}@us.ibm.com
[1]IBM T. J. Watson Research Center, 1101 Kitchawan Road, Yorktown Heights, NY 10598
Email: {deutsch, brubin, csurovic, kopcsay}@us.ibm.com
[2]IBM System and Technology Group, Boeblingen, Germany
Email: {EKLINK, WINKEL}@de.ibm.com
[3]IBM System and Technology Group, East Fishkill, NY
Email: {dpo34e, liuh, springc, dyckmanw, katopis}@us.ibm.com

Abstract

Ceramic-based wiring has been used in IBM in high-performance multi-chip module (MCM) carriers since the early 1980s. These types of carriers can provide very high wiring and power densities. Conductors are generally screened on individual ceramic sheets that are laminated and sintered at greater than 900^0 C. The high temperature process requires the use of copper paste metallization with higher resistivity than bulk copper and the punched-via fabrication imposes the use of meshed ground planes. Typical MCMs can have close to 100 layers [1] with 200–400 μm via pitch. In the case of single-chip modules (SCM), hundreds of signal I/O's on 100-200 μm pitch redistribute to the coarser module wiring. The fan-out, the hollow shielding, and the sparse and long vias generate large signal distortion and crosstalk between signal layers and via columns. This paper describes the modeling and measurement of representative glass-ceramic based wiring for both SCM and MCM applications.

Introduction

Glass-ceramic material offers lower dielectric constant (close to 5.3), lower coefficient of thermal expansion (closer to that of silicon chips), and lower sintering temperature than alumina (Al_2O_3) and thus the use of higher conductivity copper paste wiring. In addition, it offers much lower dielectric loss than typical printed-circuit-board material and therefore dielectric dispersion is very small as explained in [2]. The IBM I/P and Z-Server systems are being built using this technology because of the high-data rates that can be sustained (especially in the topmost layers) and the high wiring capacity. Due to the meshed ground planes, a quiet signal line will receive coupled noise from all the conductors in the same layer and adjacent layers above and below. The high-performance systems require data transfer on very wide buses between chips on the same carrier or between carriers with several GHz clock frequencies. The reflections from fan-out and via discontinuities, the risetime dispersion caused by resistive losses in the wiring, and noise induced distortion need to be well understood and taken into account for the design of the increasingly higher data-rate requirements. As the transmitted pulse-widths are shrinking, the probability of overlap of all the noise sources and reflections increases and the ability to maintain an adequate valid-data eye opening decreases.

Due to the complexity of the multi-layer SCM or MCM carriers, the modeling of the interconnect structure becomes very challenging and computationally intensive. This paper describes an approach to model this problem in an accurate and time-efficient extraction technique using a hybrid 2D/3D methodology based on the IBM-developed CZ2D [3-5] and EMITPKG [6-7] tools. The efficiency of the technique allows the assessment of performance impact due to processing and system tolerances by performing many sensitivity analyses. In addition, a simple time-domain technique [8] is shown for extracting the broadband complex permittivity up to 50 GHz with causally related dielectric constant, $\varepsilon_r(f)$, and dielectric loss, $\tan\delta(f)$, for the ceramic insulator and the overall losses in mesh-referenced wiring environments are discussed.

Test Vehicle

A special test vehicle was designed with representative product-level geometries and wiring configurations. The structure that was modeled and measured consisted of two signal-wiring layers, designated as R5 and R6, (with four signals each) sandwiched between three meshed reference/power layers, designated as GRD-4, GRD-5, GRD-6, as shown in Fig 1.

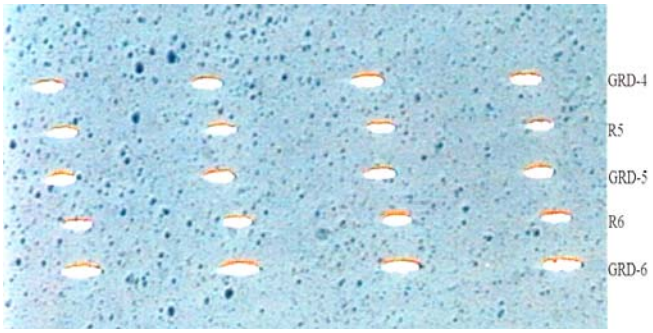

Fig. 1 Cross-sectional view of test vehicle

The signal lines, shown in Fig. 2 a), had an elliptical shape with width of 66 μm and height of 14 μm as shown in Fig. 2 b).

a)

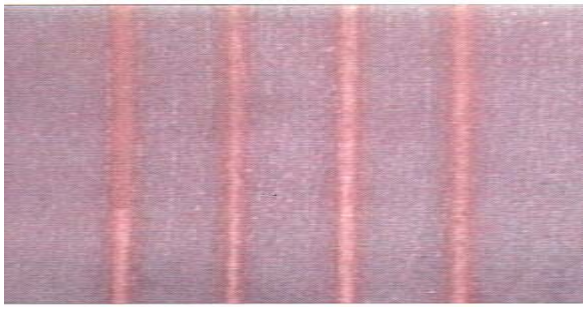

b)

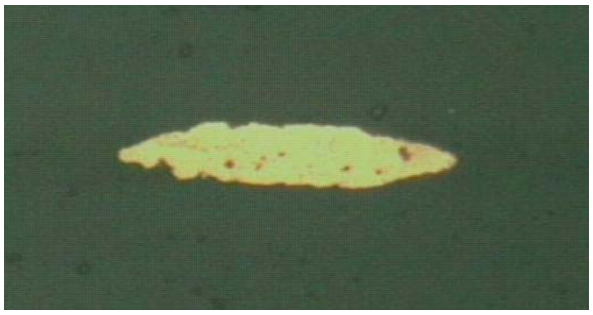

Fig. 2 a) Top –view of four signal lines, b) cross-sectional view of a signal line with elliptical shape

The pitch between the adjacent signal lines was 400 μm. Each signal line had meshed power planes directly above and below to provide the current return path as shown in Fig. 3.

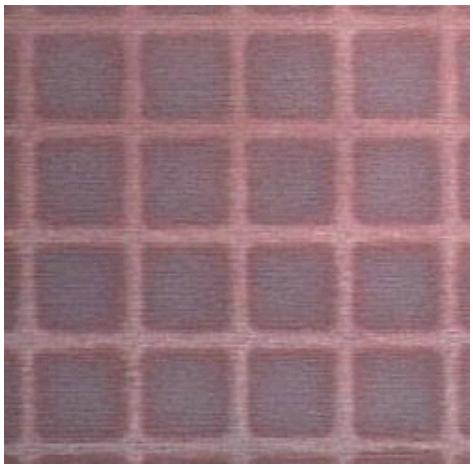

Fig. 3 Top-view of meshed power planes

The meshed power plane had width of 80 μm and thickness of 15 μm with an elliptical shape.

Modeling Methodology

The modeling involves the use of CZ2D, a highly accurate 2D quasi-static code that captures the physically correct frequency dependencies between both *C* and *G*, and between *L* and *R*, and a 3D extraction technique, EMITPKG, that captures the 3D effects caused by the mesh planes, crossing lines, and vias but can also provide the per-unit-length *R*, *L*, *C*, and *G*. The transmission line parameters are taken from the 2D analysis, but corrected for 3D effects through the application of the extraction technique on the actual structure and a 2D companion structure. This modeling flow is shown in Fig. 4 and is explained in this section.

The CZ2D code consists of a capacitance calculation routine based on the moment-method formulation described by Weeks [3], an inductance calculation routine based on another moment method formulation described by Weeks et al. [4], and a preprocessing routine that performs preliminary gridding to prepare the structure for subsequent analysis. The capacitance algorithm has been modified to include non-rectangular shapes, to include finite dielectrics through a novel technique based on boundary element and finite principles [5], and a powerful gridding algorithm that accounts for proximity and end effects. The inductance algorithm has also been modified to include non-rectangular shapes and a powerful gridding facility that accounts for proximity-, edge- and skin-effects.

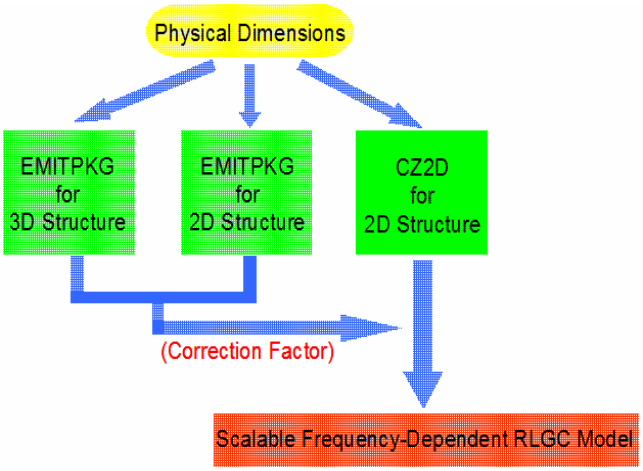

Fig. 4 Modeling Flow

The CZ2D program handles the loss tangent versus frequency for each dielectric in the structure through interpolation and use of an analytic function with self consistent real and imaginary parts, thus modeling the frequency dependent complex permittivity with real and imaginary parts that are related by a Hilbert transform. This complex permittivity is then used to calculate frequency dependent conductance, $G_{CZ2D}(f)$, and capacitance, $C_{CZ2D}(f)$. The $L_{CZ2D}(f)$ and $R_{CZ2D}(f)$ are modeled, in standard fashion, by using the CZ2D moment-method code that effectively generates and solves a parallel network of inductances and resistances. By using the same sub-sectional grid at all frequencies, the parameters generated are calculated, in effect, by the same *L*-*R* network and so must be both physically consistent and causally related.

EMITPKG uses a full-wave analysis technique [6] to calculate the *Y* parameters seen between two appropriately chosen reference planes, and from the *Y* parameters, the *RLCG* parameters per-unit-length are obtained. The procedure involves setting up a signal-line structure that is driven by sources at sufficiently far distances from the port planes that their effect on the field between the port planes is negligible. Because the calculation of *Y* parameters involves voltages and currents on the port planes [7], the effects of the regions outside the port planes are removed. Thus, EMITPKG

provides a powerful and unique method to extract the parameters of structures that resemble 2D uniform transmission lines but also include 3D effects (which precludes analysis by 2D analysis techniques).

EMITPKG is run at a single appropriate frequency, f_0, on the actual 3D structure and on a companion structure obtained by removing all those conductors that give rise to 3D effects. The same sub-sectional grid is used for both structures to remove any grid-based errors; a correction factor is thus generated as an offset between these two EMITPKG results on 3D and 2D structures as shown below.

$$R_{correction} = R_{EMITPKG\_3D}(f_0) - R_{EMITPKG\_2D}(f_0)$$
$$L_{correction} = L_{EMITPKG\_3D}(f_0) - L_{EMITPKG\_2D}(f_0)$$
$$G_{correction} = G_{EMITPKG\_3D}(f_0) - G_{EMITPKG\_2D}(f_0)$$
$$C_{correction} = C_{EMITPKG\_3D}(f_0) - C_{EMITPKG\_2D}(f_0)$$

This correction factor is then applied to parameters calculated from CZ2D as shown below.

$$R(f) = R_{CZ2D}(\text{frequency}) + R_{correction}$$
$$L(f) = L_{CZ2D}(\text{frequency}) + L_{correction}$$
$$G(f) = G_{CZ2D}(\text{frequency}) + G_{correction}$$
$$C(f) = C_{CZ2D}(\text{frequency}) + C_{correction}$$

Because the same correction factor is applied at all frequencies, the derivatives of all the parameters against frequency remain the same and thus the final parameters retain all their consistent and causal relationships.

Signal lines had elliptical shape as was shown in Fig. 2 b). In CZ2D, subsets of triangles and a rectangle were used to form an elliptical shape conductor as shown in Fig. 5. Resistivity calculated from DC measurement was used in the model.

Fig. 5 Modeled elliptical shaped conductor in CZ2D

Fig. 6 shows a snapshot of a model in EMITPKG for 3D structure with mesh planes and vias and eight coupled lines.

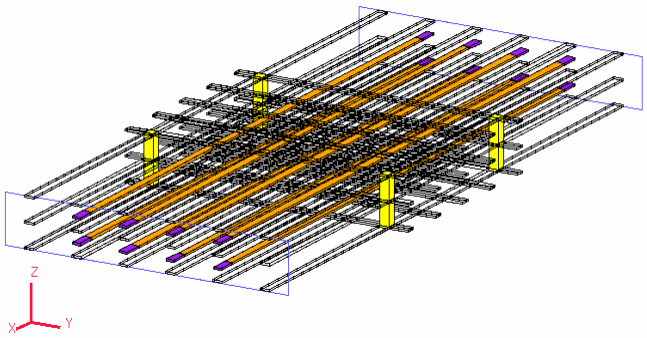

Fig. 6 Modeled 3D structure in EMITPKG

Time-Domain Characterization and Correlation with Simulation

a. Low-Frequency Measurements

The electrical properties of both the signal lines and the glass-ceramic insulator were first analyzed on a specially designed test vehicle that had single lines very close to the top surface of a large 95-mm module. These lines had reference mesh planes with 200-µm pitch above and below and very tight ground via array around the signal test pad as shown in Fig.7.

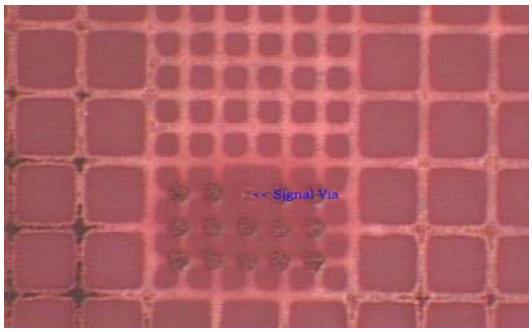

Fig. 7 Top-view of signal and ground test pads and mesh ground plane for the single-line test site.

Line lengths ranging from 0.02 to 10.28cm were included and very detailed cross sectioning was made both across the lines and along the lines. A typical cross section is shown in Fig. 8.

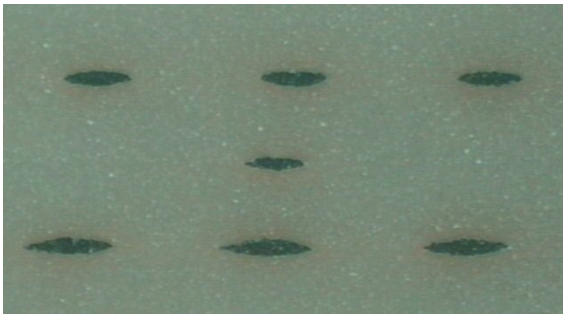

Fig. 8 Cross section of single-line site on layer six with mesh ground planes on layer five and seven.

The full characterization involves four-point resistance measurement, capacitance measurement using a low-frequency (1MHz) LCR meter, and time-domain measurement using the Agilent 86100 70GHz sampling oscilloscope. A set of lines is selected that have the same impedance and uniform cross section along the length. This screening is performed by using the 35-ps-risetime step excitation from the sampling oscilloscope and monitoring the TDR (time-domain-reflection) traces as shown in Fig. 9.

This is especially important given the elliptical cross sections shown in Figs. 2 b) and 8 with very irregular ridges. The per-unit-length resistance and capacitance is obtained by taking the difference in measured results and dividing by the difference in length. This technique eliminates the parasitic effect of vias, test pads and probes. Using the available cross sectional dimensions and measured *R* and *C*, the copper paste resistivity and dielectric constant at 1MHz are obtained.

Copper paste resistivity was found to be $\rho = 2.2$ μΩcm. The four-point line resistance measurement was also made over the temperature range -150^{0}C to +75^{0}C. It was found that the temperature coefficient of resistance was 0.36%/^{0}C which is somewhat higher than anticipated for bulk copper (around 0.31%/^{0}C). The room-temperature line resistance was measured to be R = 0.29 Ω/cm. The 1MHz line capacitance measurement was also repeated over the same temperature

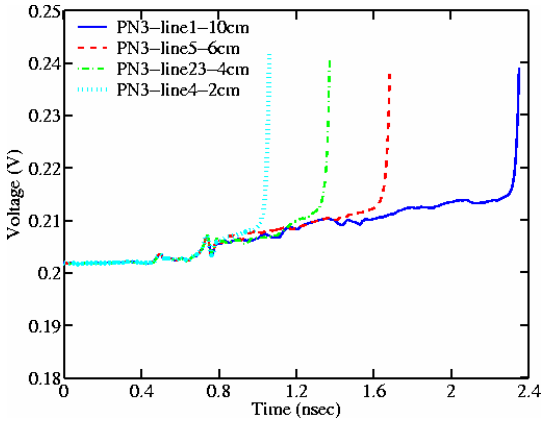

Fig. 9 TDR response on 2.016-cm, 4.012-cm, 6.008-cm, and 10.28-cm long single lines of the type shown in Fig. 8.

range and it was found that the temperature variation of the glass-ceramic dielectric constant was extremely low, namely 0.01%/^{0}C. The dielectric constant was obtained by performing modeling of the line capacitance using the CZ2D and EMITPKG tools as explained earlier. The measured and calculated line capacitance values were 1.572 pF/cm and 1.573 pF/cm, respectively, for a dielectric constant of 5.4 at 1MHz. The difference is only 0.07%.

b. Short-Pulse Propagation Measurement

The total loss and characteristic impedance of the lines were measured with a very simple time-domain technique. It employs a short, electrical pulse that is launched onto a transmission-line structure. The pulse is obtained by differentiating the step-source of the sampling oscilloscope using a passive impulse-forming network, 5206-205 manufactured by Picosecond Pulse Labs. In addition, the source risetime is improved by the use of the Picosecond Pulse Labs 4022 TDR/TDT source and 4020 pulse enhancer. The propagated pulse is recorded with the 70GHz detector of the 86118A module of the Agilent oscilloscope. High-speed coaxial probes in ground-signal (GS) configuration (GGB Industries model 40-A-250LP) were used to connect to the transmission lines. The short pulse is launched on two identical lines with lengths l_1 and l_2 and digitized by the detector. Time windowing is performed on theses pulses in order to eliminate any unwanted reflections from probes, pads, vias, and cable connectors. Since amplitude resolution is more essential than spectral resolution for time-domain measurements, rectangular windowing is used with a smooth transition to the signal baseline steady-state level. These processed waveforms are Fourier transformed, and the ratio of the complex spectra yields the propagation constant

$$\Gamma(f) = \alpha(f) + j\beta(f) = \frac{1}{l_1 - l_2}\ln\frac{A_1(f)}{A_2(f)} + j\frac{\Phi_1(f) - \Phi_2(f)}{l_1 - l_2} \qquad (1)$$

where $\alpha(f)$ and $\beta(f)$ are the frequency-dependent attenuation coefficient and phase constant, respectively. $A_i(f)$ and $\Phi_i(f)$ (i=1,2) are the amplitude and phase of the transforms corresponding to lines of lengths l_1 and l_2, respectively, with $l_1 > l_2$. No de-embedding or calibration is required since the effects of interface discontinuities simply cancel out or are eliminated by the windowing process. This is why this technique is much simpler than network-analyzer based frequency-domain methodologies. The characteristic impedance can be obtained from

$$Z_0(\omega) = \Gamma(\omega) / [\, G(\omega) + j\omega C(\omega)] \qquad (2)$$

The implicit assumption is that the measured transmission lines of lengths l_1 and l_2 have very similar characteristics and are uniform over the entire length since this extraction obtains effective per-unit-length (p.u.l.) parameters. This is why it is important to perform the screening shown in Fig. 9. Based on the cross-sectional dimensions and copper resistivity, the p.u.l. $R(\omega)$ and $L(\omega)$ were also calculated using CZ2D and EMITPKG. An initial set of values was assumed for the loss tangent of the dielectric, $\tan\delta = \varepsilon_r'' / \varepsilon_r'$ along with the real ε_r' value measured at 1MHz of 5.4. An analytic function based on the Debye model for the complex permittivity [8] was used to interpolate between the specified tanδ points.

$$\varepsilon(\omega) = \varepsilon_\infty + \sum_i \frac{\varepsilon_i}{1 + j\omega\tau_i} \qquad (3)$$

This interpolating function consists of a finite series of rational terms with self-consistent real and imaginary parts, with coefficients chosen to fit the measured total loss behavior over the desired frequency range [8]. Once an initial dielectric fit is obtained, the total measured and calculated attenuation are compared and parameters of the expansion (ε_∞, ε_i, τ_i) are adjusted to improve the fit. Two sets of short-pulse measurements were needed, namely with l_1 = 4.012 cm and l_2 = 1.008 cm, and with l_1 = 10.28 cm and l_2 = 2.016 cm. The spectral content of the two sets were 5.2 GHz – 37 GHz and 2.6 GHz - 5.3 GHz, respectively. Comparison of these two sets of data allowed us to compensate for inaccuracies caused by the imperfect cancellation of the effects of interface discontinuities when taking the ratio of the two Fourier transforms for the lines l_1 and l_2. The calculated $C(\omega)$ and $G(\omega)$ were also used to extract the frequency dependence shown in Fig.10. Here $\varepsilon_r'(\omega) = C(\omega) / C_{1MHz}$ x 5.4 and $\tan\delta(\omega) = G(\omega) / \omega C(\omega)$. This allowed the extraction of $\varepsilon_r'(\omega)$ and tanδ(ω) over the frequency range 10 KHz to 50 GHz. The high frequency range was extrapolated from 37 GHz to 50 GHz based on the behavior predicted by equation (3). Fig. 11 shows the measured and calculated total attenuation.

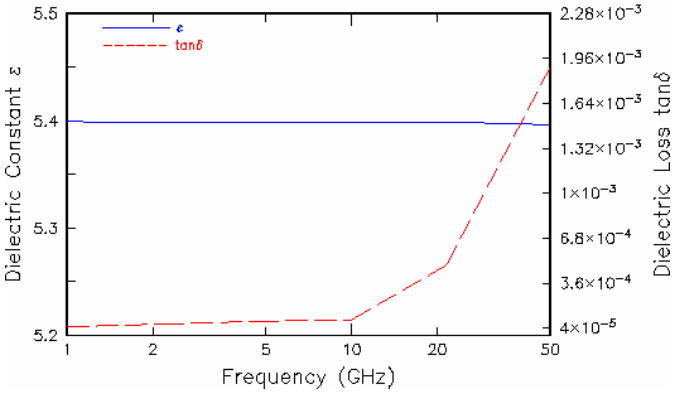

Fig. 10 Extracted dielectric constant and dielectric loss variation with frequency for glass-ceramic material.

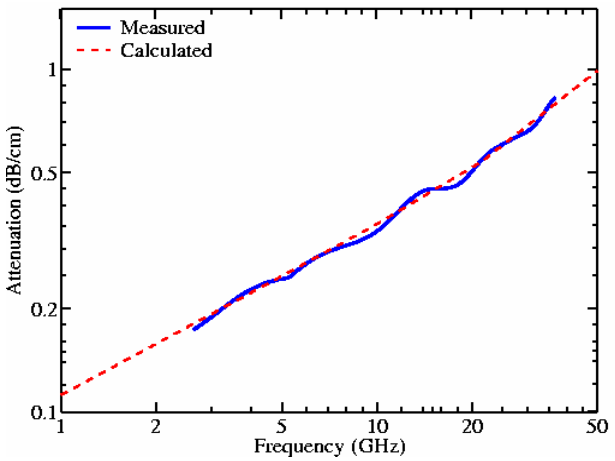

Fig. 11 Measured and calculated attenuation using the short-pulse propagation technique with 1.008-cm, 2.016-cm, 4.012-cm, and 10.28-cm long lines.

c. Signal Propagation and Crosstalk Measurements

Validation of the extracted material parameters was made by comparing the simulated and measured TDT (time-domain-transmission) and TDR waveforms. The TDR traces were used to define an equivalent model for the test pads, probes, and via discontinuities and a typical response is shown in Fig.12.

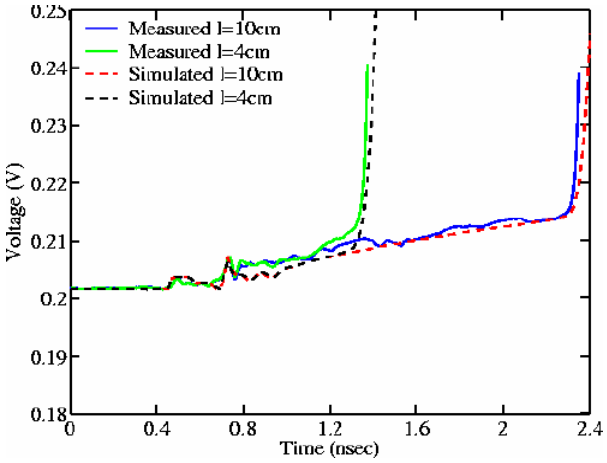

Fig. 12 Measured and simulated TDR response for 4.012-cm and 10.28-cm long lines of the type shown in Fig. 8.

A 35-ps-risetime step excitation having 202.3mV amplitude was also launched through the coaxial probes and the propagated delay, risetime dispersion, and reflection signals were measured. The 86118A 70GHz detector provides a 70 Ω termination and the signal is detected across a 55.5 Ω termination. This is why there are various steps seen in the TDT signals shown in Fig.13.

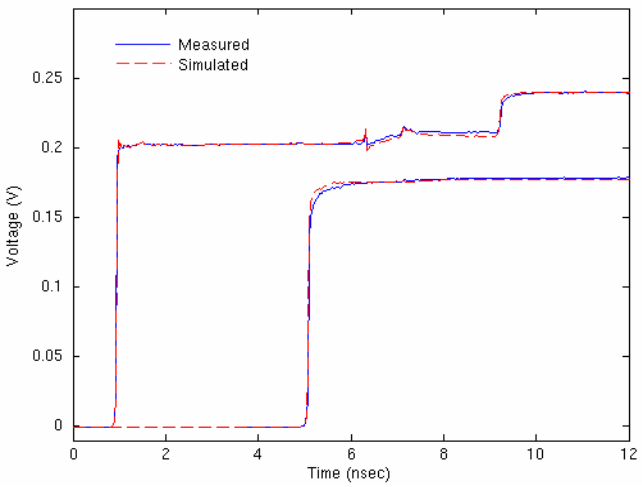

Fig. 13 Measured and simulated propagated step response for the 5.24-cm long lines on the coupled-line test site of Fig. 1.

Comparison of measured and simulated time-domain waveforms provides direct physical interpretation of the key transmission-line properties and verifies and validates the modeling technique. Fig. 14 shows the measurement set-up. TDT measurements are generally performed on several lengths of lines with an initial response taken on a 0.02016-cm lengths. The use of such a short line provides the needed reference for the longer lines to subtract the delay in the connecting cables and probes. The use of several lengths of lines is needed for both high-speed signal propagation and capacitance measurements. The propagated signal on the 0.02016cm line had 40.8 ps risetime and 186.7 mV amplitude. TABLE I shows the correlation for the 4.012 cm and 10.28 cm lines for the lines of Fig. 8. The agreement is considered quite good.

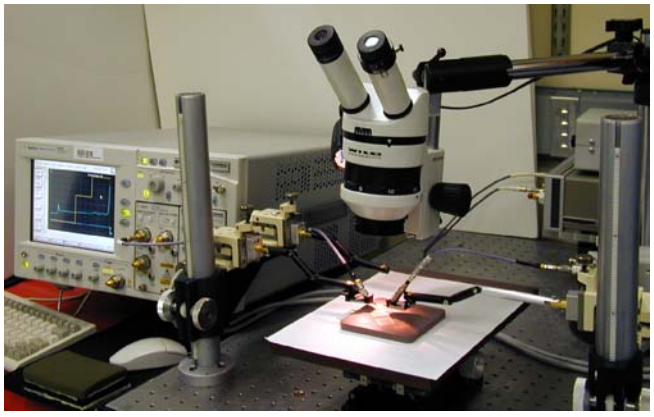

Fig. 14 Test measurement set-up showing the coaxial probes and cables connecting the test multi-chip module to the sampling oscilloscope.

Crosstalk measurements were made on the test site shown in Fig.1. Figs. 15 (vertical crosstalk), 16 (horizontal), and 17 (diagonal) show representative simulated and measured waveforms. Very good correlation is obtained even for the very small-level signals. The initial overshoot observed in the measured waveforms is believed to be caused primarily by the coupling between the long vias connecting to the coupled transmission lines. This coupling was not included in the model used for simulation.

TABLE I
Measured and Simulated Signal Propagation Results

	Voltage (mV)	Delay (ps)	Risetime (ps)
l = 4.012 cm			
Measured	185.0	323.2	160.3
Simulated	185.2	324.8	177.0
Delta (%)	+0.1	+0.5	+10.4
l = 10.28 cm			
Measured	182.0	815.9	218.0
Simulated	181.8	823.5	240.0
Delta (%)	-0.1	+0.9	+10.0

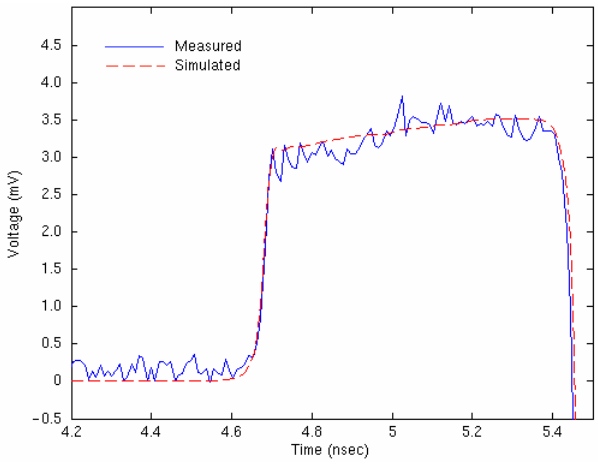

Fig. 15 Measured and simulated vertical crosstalk for the lines of Fig. 1.

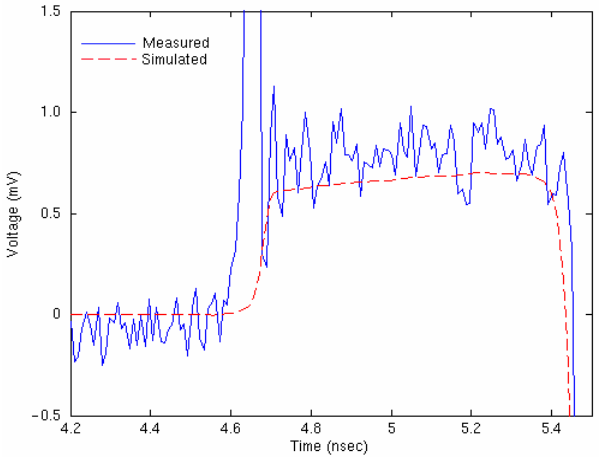

Fig. 16 Measured and simulated horizontal crosstalk for the lines of Fig. 1.

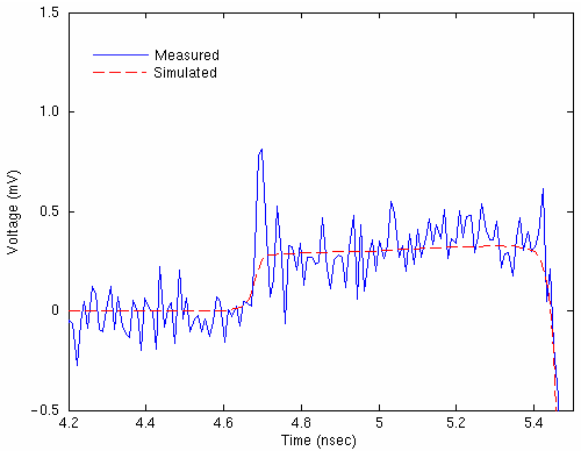

Fig. 17 Measured and simulated diagonal crosstalk for the lines of Fig. 1.

Discussion

It can be noticed in Fig.10 that the extracted tanδ for glass ceramic is quite low below 21.544 GHz (0.000098 at 10 GHz). Even at 21.544 GHz it is only 0.000488 while at 50 GHz it jumps to 0.00189. An investigation was made to assess whether the generated models omitted effects that were included in the total attenuation measured in Fig.11. First a model was built for the lines of Fig. 8 with a complete shielding box around it and no difference in the results was found when compared to the case without the shield. It was concluded that the structure was not radiating. The lines were modeled as equivalent rectangles, as ellipses similar to the ones in Fig. 5, and as ellipses with ridges as shown in Fig.18. Fig. 19 shows that the difference between the three cases is quite small. Both the elliptical shape and the ridges contribute to a slight increase in attenuation but could not account for the sharp increase in attenuation above 21.544GHz as the tanδ value suggests in Fig.10. It was found that the difference between EMITPKG_2D and EMITPKG_3D results is less than 5% up to 50 GHz. There was also very good agreement between CZ2D and EMITPKG_2D which gave confidence in the methodology.

In the range 50-70 GHz the difference in predicted loss between 2D and 3D modeling increases up to 23% while at 100 GHz there is a big jump. The height of the cross-section for the single line shown in Fig. 8 was 198 μm which approaches λ/15 for ε_r = 1 at 100 GHz (λ = 3mm). This means that the quasi-TEM assumption in the modeling could start to break down at 100 GHz and some components of the electric field could develop along the direction of propagation. The extrapolated tanδ values shown in Fig. 10 extended only to 50 GHz where the difference between 2D and 3D modeling was still less than 2%. Based on these results, it is believed that the extracted abrupt rise in tanδ above 21.544GHz is actual and reflects the real properties of the glass-ceramic material.

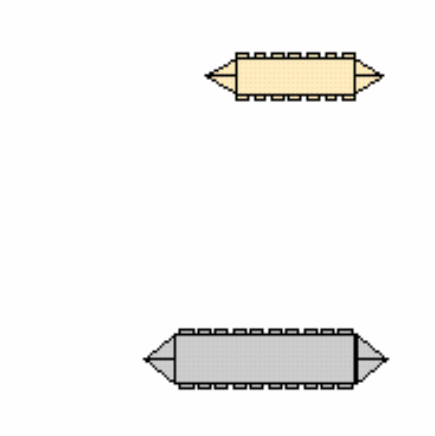

Fig. 18 Portion of model with elliptical shape and ridges shown on the signal line and the bottom mesh ground conductor.

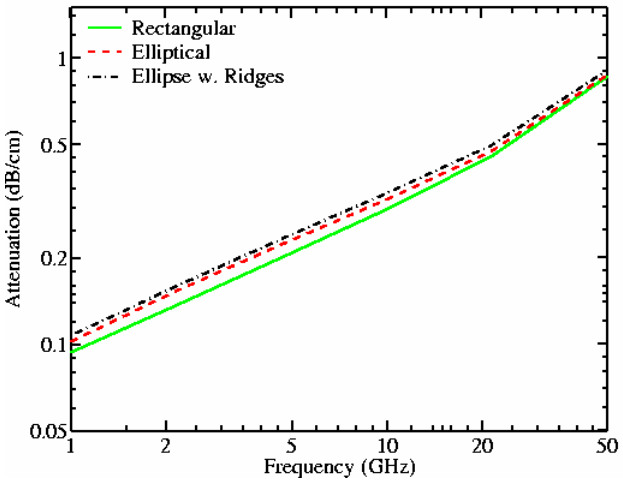

Fig. 19 Calculated attenuation with rectangular, elliptical, and elliptical with ridges (as shown in Fig. 18) cross section for the single lines of Fig. 8.

Conclusions

In this paper, an accurate and time-efficient extraction technique using a hybrid 2D/3D methodology based on the IBM developed CZ2D and EMITPKG tools was presented to model 3D wiring structure in glass-ceramic. 3D effects caused by mesh planes and vias are successfully captured by two EMITPKG runs made at a single frequency and accounted for in broadband CZ2D results as a correction factor. Simulated and measured waveform correlation showed very good agreement and thus validated the modeling method. The efficiency of the technique also allows the assessment of performance impact due to processing and system tolerances by performing many sensitivity analyses thanks to a scalable frequency dependent *RLGC* model generated using the technique. In addition, broadband dielectric constant and dielectric loss were extracted for the first time over the range 10 KHz to 50 GHz in representative multi-layer structures. The extraction was performed using a very simple time-domain technique unlike the general practice in the industry of frequency-domain extraction. The technique used allowed generation of fully-causal transmission line models up to 50 GHz. Such wide bandwidth is essential for the accurate design of multi-GHz data-rates transmitted on ceramic wiring.

References

1. George Katopis et al., "First Level Package Design Considerations for the IBM S/390 G5 Server", IEEE 7th Topical Meeting on Electrical Performance of Electronic Packaging, EPEP, pp. 15-16, October 1998.
2. Alina Deutsch, "Electrical Characteristics of Interconnections for High-Performance Systems", Proceedings of the IEEE, vol. 86, no. 2, pp. 315-355, February 1998.
3. W. T. Weeks, "Calculation of coefficients of capacitance of multiconductor transmission lines in the presence of a dielectric interface, IEEE Trans. Microwave Theory Tech.," vol. MTT-18, pp. 35-43, Jan 1970.
4. W. T. Weeks, L. L. Wu, M. F. McAllister and A. Singh, "Resistive and inductive skin effect in rectangular conductors," IBM J. Res. Develop,vol 23, no. 6, pp. 652-660, Nov. 1979.
5. A. E. Ruehli and B. J. Rubin, "Method for generating an electrical circuit comprising dielectrics", US Patent 6192507, May 1998.
6. B. J. Rubin and S. Daijavad, "Radiation and scattering from structures involving finite-size dielectric regions," IEEE Trans. Antennas Propagat., vol. 38, pp. 1863-1873, Nov. 1990.
7. B. Rubin and S. Daijavad, "Calculation of Multi-Port Parameters of Electronic Packages," IEEE 2nd Topical Meeting on Electrical Performance of Electronic Packaging, EPEP, pp. 37-39, October 1993.
8. Alina Deutsch, et al., "Extraction of $\varepsilon_r(f)$ and $\tan\delta(f)$ for Printed Circuit Board Insulators Up to 30 GHz Using the Short-Pulse Propagation Technique", IEEE Trans. On Advanced Packg., vol. 28, no. 1, pp. 1-9, Fe, 2005.